Article

The Electron Density of Bridging Hydrides Observed via Experimental and Theoretical Investigations on [Cr(μ-H)(Co)]

Piero Macchi, Daniela Donghi, and Angelo Sironi

J. Am. Chem. Soc., **2005**, 127 (47), 16494-16504• DOI: 10.1021/ja055308a • Publication Date (Web): 05 November 2005

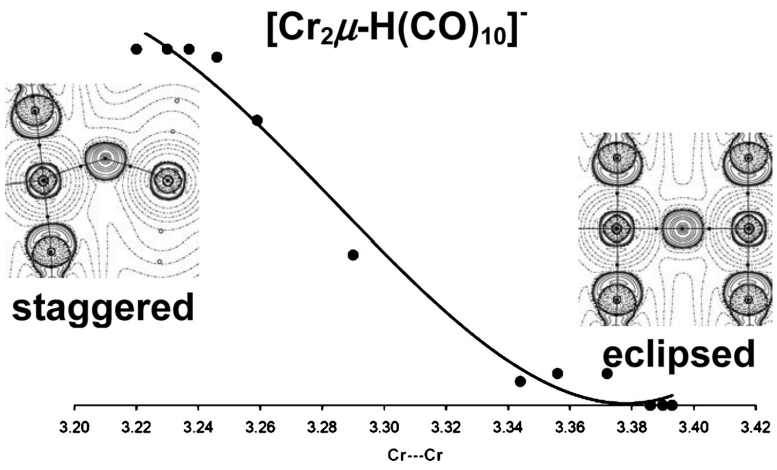

More About This Article

Additional resources and features associated with this article are available within the HTML version:

- Supporting Information
- Links to the 2 articles that cite this article, as of the time of this article download
- Access to high resolution figures
- Links to articles and content related to this article
- Copyright permission to reproduce figures and/or text from this article

View the Full Text HTML

J|A|C|S
ARTICLES
Published on Web 11/05/2005

The Electron Density of Bridging Hydrides Observed via Experimental and Theoretical Investigations on $[Cr_2(\mu_2\text{-}H)(Co)_{10}]^-$

Piero Macchi,*[†,‡] Daniela Donghi,[§] and Angelo Sironi*[†,‡]

Contribution from the Dipartimento di Chimica Strutturale e Stereochimica Inorganica, Università di Milano, via Venezian 21, 20133 Milano, Italy, CNR-ISTM, via Golgi 19, 20133 Milano, Dipartimento di Chimica Inorganica Metallorganica e Analitica, Università di Milano, Via Venezian 21, 20133 Milano, Italy

Received August 19, 2005; E-mail: piero.macchi@istm.cnr.it; angelo.sironi@istm.cnr.it

Abstract: The accurate experimental electron density distribution of $[Cr_2(\mu_2\text{-}H)(CO)_{10}]^-$ has been determined through X-ray diffraction at $T = 28$ K and gas phase theoretical calculations. The nature of the Cr−H−Cr bond has been investigated by means of the quantum theory of atoms in molecules, including the analysis of the Fermi hole distribution and the delocalization indicators from the pair density distribution. We were able to clarify not only the delocalization mechanism inside the three-center system but also the unexpected role of the equatorial carbonyls. In addition, the comparative study of a few Cr−H−X three center interactions has provided more insight into the nature of the M−H−M bond itself and has shed light on its peculiar stereochemical flexibility.

Introduction

In the past few years, the quantum theory of atoms in molecules (QTAM)[1] has become the paradigm for interpreting both the theoretical and the experimental electron density distributions. Within this framework, a link between bonding modes and topological properties has been fully achieved for "light atom" molecules. However, as we have previously shown,[2] "correspondence rules" similar to those that hold for light atoms cannot be straightforwardly extended to organometallic compounds since bonds to a transition metal display a different and much narrower spectrum of topological indexes. Here we extend our studies on the nature of metal−metal interactions (either perturbed[3,4] or unperturbed[5] by bridging carbonyls) considering the effects of the bridging hydrides.

The M−H−M bridge bond is particularly interesting to study because it is a member of a selected family, namely the electron-deficient three-center-two-electron bonds, of which the B−H−B bridge bond is perhaps the best-known example. According to the qualitative Walsh diagram outlined in Chart 1, the M−H−M moiety should be inherently bent if there is a significant M−M overlap in the M−H−M bond. In addition, one can then argue

Chart 1

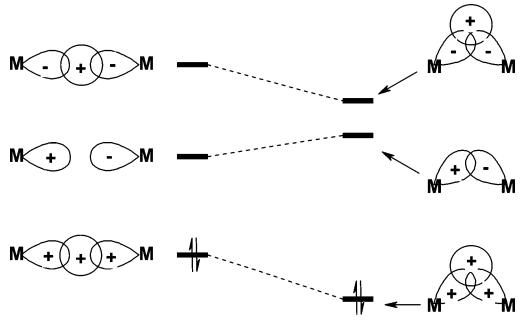

that the M−H−M system would prefer to remain bent and not to place an additional two electrons into the mid-energy orbital. If forced to do so, the M−H−M would revert into a linear electron-rich three-center-four-electron bond which is most likely unstable with respect to dissociation into (M−H + M) fragments.[6] Noteworthy, the fact that a three-center-two-electron bond implies the presence of some M−M bonding should not be taken to mean that there are separate M−M and M−H bonds.

A common corollary to the above picture was to consider the M−H−M system as a "protonated metal−metal bond,[7,8] since it may be formally derived from the protonation of the M−M bonding electron pair of the "parent" compound (i.e. $[Cr_2(CO)_{10}]^{2-}$ in the case of $[Cr_2(\mu_2\text{-}H)(CO)_{10}]^-$). Presently, M−H−M complexes can be better considered as σ complexes

† Dipartimento di Chimica Strutturale e Stereochimica Inorganica, Università di Milano.
‡ CNR-ISTM.
§ Dipartimento di Chimica Inorganica Metallorganica e Analitica, Università di Milano.

(1) Bader, R. F. W. *Atoms in Molecules: A Quantum Theory*; Cambridge University Press: Oxford, UK, 1991.
(2) Macchi, P.; Sironi, A. *Coord. Chem. Rev.* **2003**, *238/239*, 383−412.
(3) Macchi, P.; Garlaschelli, L.; Martinengo, S.; Sironi, A. *J. Am. Chem. Soc.* **1999**, *121*, 10428−10429.
(4) Macchi, P.; Garlaschelli, L.; Sironi, A. *J. Am. Chem. Soc.* **2002**, *124*, 14173−14184.
(5) Macchi, P.; Proserpio, D. M.; Sironi, A. *J. Am. Chem. Soc.* **1998**, *120*, 13429.
(6) Bau, R.; Teller, R. G.; Kirtley, S. W.; Koetzle, T. F. *Acc. Chem. Res.* **1979**, *12*, 176−183.
(7) (a) Handy, L. B.; Treichel, P. M.; Dahl, L. F.; Hayter, R. G. *J. Am. Chem. Soc.* **1966**, *88*, 366. (b) Handy, L. B.; Ruff, J. K.; Dahl, L. F. *J. Am. Chem. Soc.* **1970**, *92*, 7312.
(8) *Advanced Inorganic Chemistry: A Comprehensive Text*, 4th ed.; Cotton, F. A., Wilkinson, G., Eds.; J. Wiley & Sons: New York, 1980; p 1116.

10.1021/ja055308a CCC: $30.25

of an M−H bond.[9,10] The synthetic consequences of the σ-bond concept were successfully exploited by Venanzi who synthesized a series of new M−H−M complexes from the reaction of various metal hydrides with coordinatively unsaturated metal complex fragments.[11]

It is now well established that mononuclear transition metal hydrides have a strong tendency to form di- or polynuclear assembles containing M−H−M structural units and much work has been carried out to clarify their structure, reactivity, spectroscopy and bonding properties.[12,13] However, to the best of our knowledge, no previous, theoretical or experimental, charge density study has been reported on these systems.[14] Here we fill the gap reporting and discussing the electron density distribution of the $[Cr_2(\mu_2\text{-H})(CO)_{10}]^-$ anion as obtained from both an accurate X-ray diffraction experiment on a single crystal of the $[K(crypt\text{-}222)][Cr_2(\mu_2\text{-H})(CO)_{10}]$ salt and quantum chemical computations.

Experimental Section

Preparation of $[K(crypt\text{-}222)][Cr_2(\mu_2\text{-H})(CO)_{10}]$. All the manipulations were performed under N_2 using oven dried Schlenk-type glassware. C_2H_5OH (Fluka) was deoxygenated and dried on activated molecular sieves; THF (Aldrich) was distilled on Na/benzophenone before using. $Cr(CO)_6$, KBH_4, and $C_{18}H_{36}N_2O_6$ (crypt-222) were purchased by Aldrich and used as received. IR spectra were acquired on a Bruker vector 22 FT spectometer.

The $[K(crypt\text{-}222)]^+$ salt was prepared following the literature method.[15] To a Schlenk tube containing 240 mg of $Cr(CO)_6$ (1.09 mmol) and 40 mg (0.74 mmol) of KBH_4 were added 15 mL of freshly distilled THF. The mixture was refluxed for 24 h and then filtered to remove the excess KBH_4. The filtered red solution was dried under vacuum and treated with 200 mg of (crypt-222) (0.53 mmol) dissolved in 10 mL of absolute ethanol freshly distilled. The solution was put at 248 K. After 5 days red crystals (of $[K(crypt\text{-}222)]_2[Cr_2(\mu_2\text{-H})(CO)_{10}][HCr(CO)_5]$)[16] had formed, leaving a yellow solution. The solution was separated from the crystal and left at 248 K, which gave yellow big crystals of $[K(crypt\text{-}222)][Cr_2(\mu_2\text{-H})(CO)_{10}]$ in few days. IR for the yellow crystals (CH_2Cl_2): ν_{CO} = 2031 w, 1938 vs, 1871 s.

X-ray Data Collection and Model Refinements. A suitable $[K(crypt\text{-}222)][Cr_2(\mu_2\text{-H})(CO)_{10}]$ yellow crystal of approximately spherical shape (ca. 0.2 mm diameter) was selected, mounted on a goniometer head and cooled to 28 K at −2 K/min. A Bruker SMART-CCD diffractometer, equipped with the Oxford Cryosystem HELIX, was used for data collection. The crystal was left more than 2 h at the minimum temperature to let it to equilibrate; in fact, a previous test on a phase transition crystal demonstrated that at least 1 h is necessary before an equilibrium is reached at the same temperature measured inside the HELIX nozzle. Temperature was hereinafter stable at 28 K within 0.1 K.

The detector was positioned in three different θ settings (0°, 35°, 65°) with detector−sample distance of 3.85(1) cm (shorter detector−sample distances are hampered by the HELIX nozzle). The scan axes were either ω and ϕ, with scan width of 0.3°. Eight runs were carried out with acquisition time/frame of 30, 60, and 90 s for the three different θ settings, respectively. Two extra runs at $2\theta = -65°$ were measured after a few hours on the same crystal at the same temperature and orientation. No scaling problems were detected for the two extra runs while correcting and merging the datasets.

A total of 128 749 intensities were collected, 804 of which were discarded because of being partially obscured by the beam stop or the beam stop arm. The 127 945 good intensities were then corrected for diffraction anisotropies and crystal absorption and merged to 30 760 unique reflections with the program SORTAV (267 intensities were judged as outliers and thus rejected, systematic absences and negative F^2 were excluded, $R_{merge} = 0.039$). Completeness was 100% up to sin $\theta/\lambda = 0.71$ Å^{-1} and 87% up to $(\sin\theta/\lambda)_{max} = 1.052$ Å^{-1}. No intensity decay was observed at the end of the 4-day data collection.

The XD code[17] was used for the multipolar refinements, using the Hansen and Coppens pseudoatomic expansion:[18]

$$\rho(\mathbf{r}) = \sum_{i=1}^{N} \rho_i(\mathbf{r} - \mathbf{r}_i)$$

$$\rho_i(\mathbf{r}_i) = P_{ic}\rho_{core}(\mathbf{r}_i) + \kappa'^3\rho_{valence}(\kappa\mathbf{r}_i)P_{iv} + \sum_{l=0}^{4}[\kappa'^3 R_l(\kappa\mathbf{r}_i)\sum_{m=0}^{l} P_{ilm\pm}y_{lm\pm}(\mathbf{r}_i/r_i)]$$

Relativistic atomic wave functions[19] were adopted for describing core and spherical valence. Cr atoms were expanded up to the hexadecapole level; C, N, and O atoms, up to the octopole level; the K atom was considered as a spherical ion; H atoms were expanded up to the quadrupole level, after fixing their positions and anisotropic thermal factors at those determined from a neutron diffraction experiment at 20 K, known from the literature.[15] A comparison of thermal parameters of non-H atoms obtained from our X-ray experiment compare quite well with those of the neutron study ($\langle U_{eq}(\text{neutron})\rangle/\langle U_{eq}(\text{X-ray})\rangle$ = 0.98(2); the average discrepancy of each principal component of the **U** tensors is 12%). For this reason, no scaling for the **U** tensors of H atoms (as determined by neutrons) was judged necessary. The radial part of the deformation densities were constructed from single-ζ Slater type orbitals[20] for C, N, O (with n_l = 2,2,2,3), H (n_l = 0,1,2) and from 3d orbitals for Cr.[19] κ and κ' radial scaling parameters were refined for each "chemically" independent atom (one Cr, two O's, two C's, one N; two H's). For oxygens, κ' was fixed equal to κ to avoid unrealistic expansions.[21] For Cr κ and κ' were constrained to be equal, given that the same radial functions are used for spherical valence monopole and higher multipoles. To reduce the number of variables, hydrogen atoms of the crown ether were modeled with just one dipole and one quadrupole (directed toward C−H bond), while a full set of dipole and quadrupole coefficient was refined for the hydridic H.

The quantity minimized was $\epsilon = \sum w(F_o - F_c)^2$ based on the 20 964 reflections with $F > 3\sigma(F)$; weights were always taken as $w = 1/\sigma^2(F)$. Convergence was assumed when $|\delta\mathbf{x}|/\sigma(\mathbf{x}) < 0.01$ for each variable. No significant extinction was found. A residual of 0.65 e/Å^3 was found at 0.7 Å from the K cation, probably due to some anharmonic motion

(9) Crabtree, R. H. *Angew. Chem., Int. Ed. Engl.* **1993**, *32*, 789−805.
(10) *The Organometallic Chemistry of the Transition Metals*; Crabtree, R. H. Wiley-VCH: New York, 1994.
(11) Venanzi, L. M. *Coord. Chem. Rev.* **1982**, *43*, 251−274.
(12) Dedieu, A., Ed. *Transition Metal Hydrides*; Wiley-VCH: New York, 1992.
(13) Peruzzini, M., Poli, R., Eds. *Recent Advances in Hydride Chemistry*; Elsevier: Amsterdam, New York, 2001.
(14) A study of Si−H−Mn systems is reported by Bader, R. F. W.; Matta, C. F.; Cortés-Guzmán, F. *Organometallics* **2004**, *23*, 6253−6263; a paper about M−M bond protonation in unsaturated dimers has been recently submitted for publication by Dr. C. Mealli and co-workers (personal communication).
(15) Petersen, J. L.; Brown, R. K.; Williams, J. M. *Inorg. Chem.*, **1981**, *20*, 158−165.
(16) The structure, which is not reported here, was solved by single-crystal X-ray diffraction (unit cell parameters: a = 18.14(1) Å, b = 17.898(8) Å, c = 21.99(1) Å, β = 86.58(2)°, V = 7128(11) Å^3; space group $P2_1/c$).
(17) Koritsanszky, T.; Howard, S. T.; Richter, T.; Macchi, P.; Volkov, A.; Gatti, C.; Mallinson, P. R.; Farrugia, L. J.; Su, Z.; Hansen, N. K. *XD*, A computer program package for multipole refinement and topological analysis of charge densities from diffraction data; Free University of Berlin: Berlin, Germany, 2003.
(18) Hansen, N. K.; Coppens, P. *Acta Crystallogr., Sect. A* **1978**, *34*, 909−921.
(19) (a) Su, Z.; Coppens, P. *Acta Crystallogr.* **1998**, *A54*, 646−652. (b) Macchi, P.; Coppens, P. *Acta Crystallogr.* **2001**, *A57*, 656−662.
(20) Clementi, E.; Raimondi, D. L. *J. Chem. Phys.* **1963**, *38*, 2686−2689. For sp shell, the exponents of 2s and 2p orbitals are simply averaged.
(21) Abramov, Y.; Volkov, A.; Coppens, P. *Chem. Phys. Lett.* **1999**, *311*, 81−86.

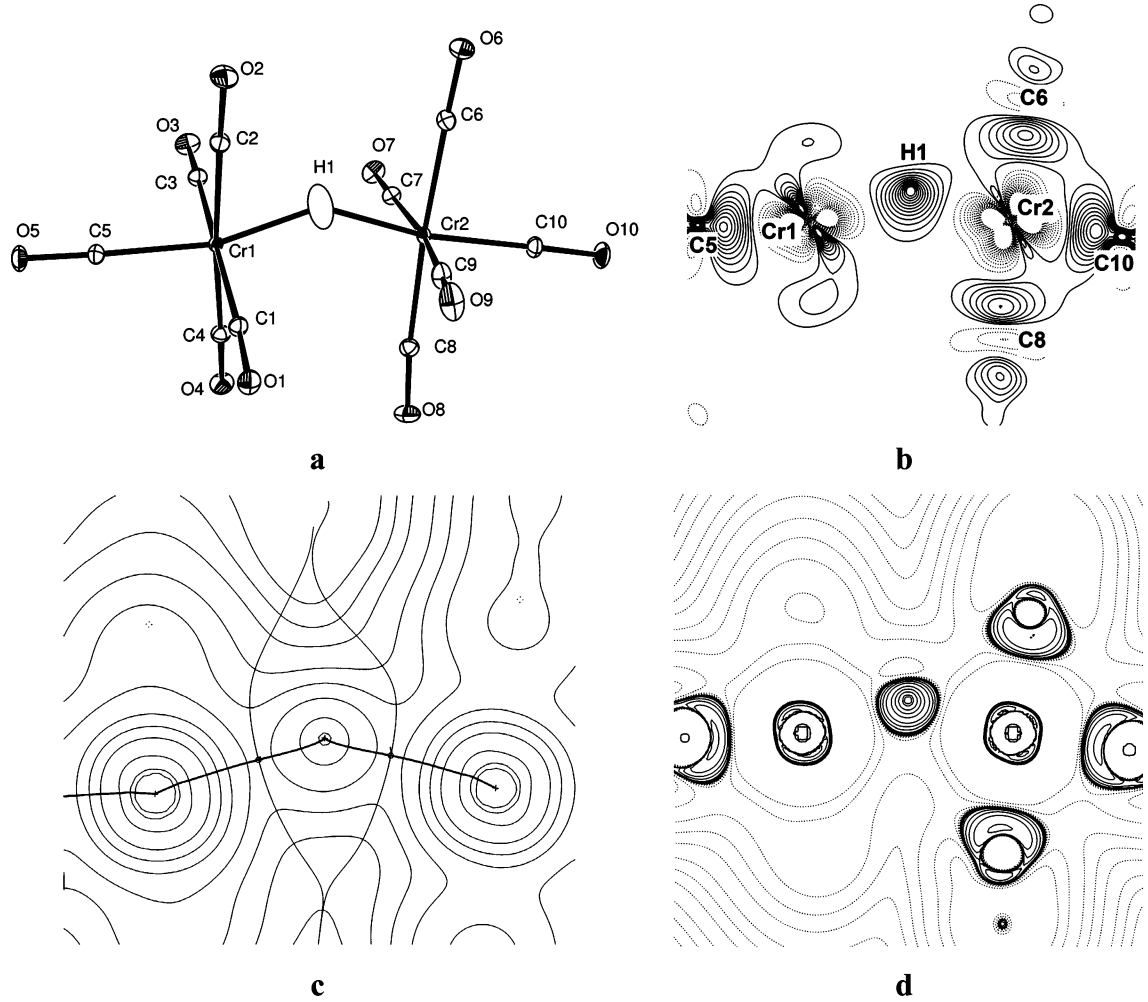

Figure 1. (a) ORTEP representation of $[Cr_2(\mu_2\text{-H})(CO)_{10}]^-$ anion with ellipsoids drawn at 50% probability level (anisotropic thermal parameters for H were taken from the neutron diffraction study).[15] (b) Static deformation density in the Cr−H−Cr plane (note that equatorial carbonyls coordinated to Cr(2) lie approximately on this plane, while those coordinated to Cr(1) are somewhat shifted); contours are drawn at ±0.05 eÅ^{-3}, solid contours are positive values, dotted contours are negative. (c) Total electron density distribution in the same plane (contours are drawn at 1.0, 2.0, 4.0, 8.0 × 10^x, $x = -2, -1, 0, +1$ eÅ^{-3}); Cr(1)−H and Cr(2)−H bond paths and interatomic surfaces are superimposed. (d) $\nabla^2\rho(\mathbf{r})$ distribution in the same plane (contours drawn at ± 1.0, 2.0, 4.0, 8.0 × 10^x, $x = -2, -1, 0, +1$ eÅ^{-5}; negative contours are solid lines, positive contours are dotted lines).

or slight static disorder induced by the weak potential experienced by this atom, which is quite at variance from the usual tight binding of an alkaline cation in ionic salts.[22] Different data reduction and correction procedures always ended up with this feature. A similar residual in the same position was observed also after refining a model from a 90 K experiment (reported elsewhere)[23] performed on another crystal, which reinforces the hypothesis that this feature is due to some atypical motion of the K atom (unavoidable even at 28 K). By including an anharmonic motion treatment for the K atom, an electron density model not significantly different was refined for the rest of the crystal, and the highest residual peak in the vicinity of K was reduced below 0.45 e/Å^3. If we consider the low-order data only (sin $\theta/\lambda < 0.7$ Å^{-1}), the highest residual peak is 0.22 e/Å^3, which ensures that valence electrons are quite well accounted for all over the structure and that the error is quite localized in a region of no interest for our purposes. In fact, no special residual feature is observed in the anion molecule, and the rms residual density in the whole unit cell is quite low in both models with and without anharmonic motion (0.077 and 0.078 e/Å^3, respectively). A residual density map in the plane Cr−H−Cr is reported in the Supporting Information. A representation of the anion geometry is shown in Figure 1a. Crystallographic data and further details of the multipolar refinements are listed in Table 1.

In this paper, the electron density of the $[K(crypt\text{-}222)]^+$ cation is not discussed, but we can simply mention that analyses of thermal parameters (rigid body test) and topological indexes give results in agreement with expectation, confirming the good quality of the experiment.

Theoretical Calculations. All molecular orbital computations were performed using GAUSSIAN03.[24] The density functional theory at B3LYP[25] and BP86[26] levels was used for geometry optimization. Basis sets adopted were: (1) relativistic small-core effective core potentials[27] with a basis set splitting (341/311/41) for the metals and double-ζ quality[28] all-electron basis (721/41) for C and O with two polarization *d* functions on C and O (basis set *ecp*), (2) all electron basis set of 6-311++G quality for both the second row elements and the metals, including one polarization *d* function for second row atoms and one *f* function for the metals (*ae*).

(22) In $[Cr_2(\mu_2\text{-H})(CO)_{10}][K(crypt\text{-}222)]$ there is an extra volume of about 7 Å^3 available per each K atom in the unit cell (evaluated using standard van der Waals radii and a 1.1 Å sphere as a probe).

(23) Macchi, P.; Sironi, A. *Acta Crystallog.* **2004**, *A60*, 502−509.
(24) Frisch, M. J. et al. *Gaussian 03*, revision B.01; Gaussian, Inc.: Pittsburgh, PA, 2003.
(25) (a) Becke, A. D. *J. Chem. Phys.* **1993**, *98*, 5648−5652. (b) Lee, C.; Yang, W.; Parr, R. G. *Phys. Rev. B* **1988**, *37*, 785−789.
(26) (a) Becke, A. D. *Phys. Rev. A* **1988**, *38*, 3098−3100. (b) Perdew, J. P. *Phys. Rev. B* **1986**, *33*, 8822−8824.
(27) Hay, P. J.; Wadt, W. R. *J. Chem. Phys.* **1985**, *82*, 299.
(28) Dunning, T. H.; Hay, P. J. *Modern Theoretical Chemistry*; Schaefer, H,. F., III, Ed; Plenum: New York, 1976; Vol. 3, p 1.

Table 1. Crystallographic Data for $[K(crypt\text{-}222)][Cr_2(\mu_2\text{-}H)(CO)_{10}]$, Summary of Data Collection and Residual Indexes after Multipolar Refinement

cmpd	$[K(crypt\text{-}222)][Cr_2(\mu_2\text{-}H)(CO)_{10}]$
instrument	SMART CCD
T (K)	28(2) K
a (Å)	10.4580(4)
b (Å)	14.4168(5)
c (Å)	23.882(1)
β (°)	97.264(3)
V (Å^3)	3571.8(3)
λ (Å)	0.7107
max $\sin(\theta)/\lambda$ (Å^{-1})	1.06
space group	$P2_1/c$
intensities collected	128749
unique reflections	30760
R_{int}	0.0391
R_σ	0.0446
included in the refinement ($F > 3\sigma(F)$)	20964
residual after multipolar refinement: (in parentheses indexes of the model with anharmonic motion included for K^+)	
$R_1(F > 3\sigma(F))$	0.0263 (0.0262)
R_1(all reflections)	0.0729 (0.0729)
$R_2(F > 3\sigma(F))$	0.0339 (0.0335)
R_2 (all reflections)	0.0429 (0.0425)
wR_1	0.0206 (0.0204)
wR_2	0.0399 (0.0395)
gof	1.21 (1.20)

Topological properties of the SCF and Khon−Sham electron densities were investigated with the programs AIMPAC,[29] AIM2000,[30] MORPHY98,[31] and local routines to compute the delocalization indexes. The program XAIM[32] was used to produce Fermi hole maps.

Results and Discussion

$[Cr_2(\mu_2\text{-}H)(CO)_{10}]^-$ Experimental vs Theoretical Geometries. The structure of the $[Cr_2(\mu_2\text{-}H)(CO)_{10}]^-$ anion, as observed in its $[K(crypt\text{-}222)]^+$ salt, is highlighted in Figure 1a. This particular salt was chosen because the anion does not sit at a special position and because a preexisting neutron diffraction study (at 20 K) was available,[15] thus allowing a correct treatment of the hydride ligand in our refinements.

The chiral $[K(crypt\text{-}222)]^+$ cation was originally (in the late 1970s) and successfully selected because its maximal attainable symmetry (D_3) does not match with that of the anion (either D_{4h} or D_{4d}), thus increasing the probability of finding an ordered anion with a low-symmetry conformation. Since then, many other ordered $[Cr_2(\mu_2\text{-}H)(CO)_{10}]^-[X]^+$ salts have been structurally characterized, but none of them has been studied by low-temperature neutron diffraction. A collection of the pertinent bond lengths comparing the neutron (at 20 K from ref 15) and the X-ray (at 28 K, from this study) diffraction experiments is reported in Table 2.

In the $[K(crypt\text{-}222)]^+$ salt, the $[Cr_2(\mu_2\text{-}H)(CO)_{10}]^-$ anion is ordered and adopts a slightly bent conformation which is intermediate between the linear, eclipsed conformation found in the PPN salt[33] and the bent, staggered conformation found in the $[Cu(PPh_3)_3]^+$ salt.[34] Despite the early claims concerning the observation of a linear Cr−H−Cr fragment in the $[NEt_4]^+$ salt,[35] it is now well assessed that the M−H−M angles are invariably (more or less) bent.[36] This is confirmed not only by a few neutron diffraction evidences but also by gas-phase theoretical geometry optimizations (vide infra) and by geometrical considerations on the more abundant X-ray diffraction studies. Indeed, assuming that the M−H bond distance is essentially constant (within hundreds of Å) in eclipsed and staggered derivatives, it is clear that even the longest M···M distances determined are shorter than the sum of two M−H bonds. Within the above assumption, the M−H−M angles can be estimated also for X-ray determined structures, using the Carnot theorem,[37] see results summarized in Figure 2.

Table 2. Principal Interatomic Distances from the X-ray (this work) and Neutron Experiments[15]

	neutron 20 K	X-ray 28 K		neutron 20 K	X-ray 28 K
Cr1−Cr2	3.300(4)	3.305(1)	Cr2−H	1.723(5)	1.728[a]
Cr1−H	1.735(5)	1.734[a]	Cr2−C6	1.899(3)	1.8997(8)
Cr1−C1	1.900(3)	1.8995(6)	Cr2−C7	1.895(3)	1.8964(6)
Cr1−C2	1.903(4)	1.9043(7)	Cr2−C8	1.898(3)	1.8964(8)
Cr1−C3	1.897(3)	1.8982(7)	Cr2−C9	1.907(3)	1.9093(7)
Cr1−C4	1.899(4)	1.8964(7)	Cr2−C10	1.851(3)	1.8454(6)
Cr1−C5	1.846(3)	1.8490(7)	C6−O6	1.147(3)	1.147(1)
C1−O1	1.148(2)	1.152(1)	C7−O7	1.145(3)	1.152(1)
C2−O2	1.145(3)	1.149(1)	C8−O8	1.145(3)	1.151(1)
C3−O3	1.143(3)	1.150(1)	C9−O9	1.142(3)	1.147(1)
C4−O4	1.143(3)	1.151(1)	C10−O10	1.161(3)	1.161(1)
C5−O5	1.159(3)	1.159(1)			

[a] Hydrogens fixed as in the neutron study (standard uncertainty omitted for this parameter)

The point where the hydrogen's and the metals' orbitals "ideally" overlap can be tentatively located at the intersection of the two axial ligand metal vectors (see Chart 2). According to these estimations, whatever the conformation of the $[Cr_2(\mu_2\text{-}H)(CO)_{10}]^-$ anion, the H atom is always found in a characteristically bent, off-axis position well above the ideal intersection of the orbitals.

Thus, *from a geometrical point of view*, one could argue a *closed* 3-center-2-electron bond (3c-2e). This implies the occurrence of some "direct" M- - -M bonding, which should be detectable in the features of the electron density or, at least, of the pair density.

Organometallic species are known to be rather flexible, and the actual value of angles and distances to a metal quite severely depends on the intermolecular environment.[39] Judging from the variability of conformations observed for the $[Cr_2(\mu_2\text{-}H)(CO)_{10}]^-$ anion (see Figure 2), it is clear that the Cr−H−Cr moiety is interconnected by one of the most flexible organometallic

(29) Biegler-König, F. W.; Bader, R. F. W.; Ting-Hua, T. *J. Comput. Chem.* **1982**, *3*, 317−328.
(30) Biegler-König, F. W. *AIM2000*, version 2.0, University of Applied Sciences: Bielefeld, Germany, 2000.
(31) Popelier, P. L. A. *Comput. Phys. Commun.* **1996**, *93*, 212−240; Popelier, P. L. A. *Chem. Phys.* **1994**, *228*, 160−164.
(32) Ortiz Alba, J. C.; Bo, C. *Xaim-1.0*; Universitat Rovira I Virgili: Tarragona, Spain; http://www.quimica.urv.es/XAIM.
(33) (a) Petersen, J. L.; Johnson, P. L.; O'Connor, J.; Dahl, L. F.; Williams, J. M. *Inorg. Chem.* **1978**, *17*, 3460−3469. (b) Petersen, J. L.; Brown, R. K.; Williams, J. M.; McMullan, R. K. *Inorg. Chem.* **1979**, *18*, 3493−3498.
(34) Klufers, P.; Wilhelm, U. *J. Organomet. Chem.* **1991**, *421*, 39−54.
(35) (a) Handy, L. B.; Treichel, P. M.; Dahl, L. F.; Hayter, R. G. *J. Am. Chem. Soc.* **1966**, *88*, 366−367. (b) Handy, L. B.; Ruff, J. K.; Dahl, L. F. *J. Am. Chem. Soc.* **1970**, *92*, 7312−7326.
(36) The original misunderstanding was due to the fact that, for long Cr···Cr distances, the eclipsed $(CO)_5$ Cr···Cr$(CO)_5$ moiety is substantially centrosymmetric (despite the presence of a bent Cr−H−Cr angle), thus promoting the disordering of the $[Cr_2(\mu_2\text{-}H)(CO)_{10}]^-$ anion about a crystallographic inversion center (as later observed for most of the eclipsed derivatives).
(37) Honsberger, R. *Mathematical Gems III*; Mathematical Association of America: Washington, DC, 1985; p 25.
(38) Grillone, M. D.; Benettollo, F.; Bombieri, G.; Del Pra, A. *J. Organomet. Chem.* **1999**, *575*, 193−199.
(39) Martin, A.; Orpen, A. G. *J. Am. Chem. Soc.* **1996**, *118*, 1464−1470.

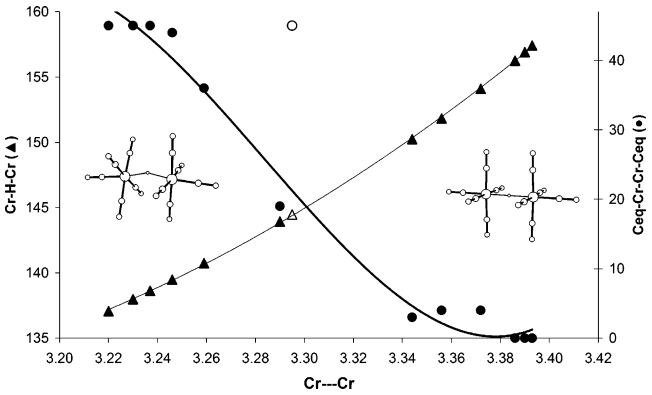

Figure 2. Scatter plot of the Cr−H−Cr (triangles) and C_{eq}−Cr−Cr−C_{eq} (circles) angles vs the Cr···Cr distance. The Cr−H−Cr bond angles have been computed with the Carnot theorem, assuming a constant Cr−H bond distance of 1.73 Å, from the Cr···Cr distance. The empty circle and triangle refer to the structure of the $[K(phen)_2]^+$ salt where both the cation and the anion lie on a mirror plane. For this complex the moderately large *U* factor of the equatorial carbonyls bound to Cr_1 could hide some disorder, thus justifying the "anomalous" C_{eq}−Cr−Cr−C_{eq} angle.[38]

Chart 2

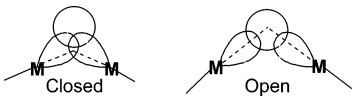

bonds.[40] This is confirmed also by density functional computations that estimate the energy difference between the staggered and the eclipsed conformation to be smaller than 2.0 kcal mol^{-1} despite being associated to a large geometrical variation (which, in addition, depends on the chosen gradient correction method).[41] These considerations reasonably hold also for all M−H−M fragments which are very likely associated always with a rather flat potential energy surface.

We report in Figure 3 and Table 3 the most relevant stationary points of the potential energy surface (PES) of the $[Cr_2(\mu_2\text{-H})(CO)_{10}]^-$ anion at the DFT-B3LYP or DFT-BP86 level (as previously observed,[41] the nonlocal BP86 functional seems to better reproduce experimental geometries). By comparing Figures 2 and 3 and focusing on the carbonyls, it is clear that the "reaction path" outlined by the structure correlation principle[42] concerns the conversion of a staggered (**S**) conformer into an eclipsed (**E**) one. A full theoretical investigation of the PES tells us that actually there are three kinds of **S** stationary points (see Supporting Information for more details): the Cr−H−Cr moiety is linear for one of these (D_{4d}) but bent for the others (C_2 and C_s). In the C_s conformer, the Cr−H−Cr mirror plane is eclipsed to one $Cr(CO)_5$ moiety but staggered to the other. Most theoretical methods predict C_s to be more stable (quite substantially with respect to D_{4d}, but only by less than 0.05 kcal/mol against C_2) and to be a true minimum on the PES.[43] Moreover, from the experimental structures we observe that all (but one) "staggered" anions have the hydride ligand substantially eclipsed with respect to a nearby carbonyl. Also for the eclipsed isomers, at the BP86 level, we found three stationary points: two have Cr−H−Cr < 180° and C_{2v} symmetry (they differ only in the staggered or eclipsed nature of the hydride with respect to the equatorial carbonyls), and one has a linear Cr−H−Cr and therefore D_{4h} symmetry.[44] From data reported in Table 3 we can infer that to reach the D_{4h} stationary point (a minimum at BP86/*ae* while a second-order saddle at BP86/*ecp*) from the C_s one, at least two kinds of paths are possible: one starts with the Cr−H−Cr "linearization" (i.e. approaching the D_{4d} second-order saddle); the other, instead, is first associated with the eclipsing of the carbonyls (i.e. the C_{2v} geometry).[45] From the theoretical calculations, the former is expected to be of lowest energy (at least slightly), but the experimentally derived one is very similar to the latter, leading to a pseudo C_{2v} conformer, whose "asymptotic" limit would be the predicted D_{4h} structure.[46] Since all **E** conformers are higher in energy than those of **S**, we can just observe that the well-known rule of thumb that long hydrido-bridged M−M bonds have (invariably) eclipsed carbonyls does not hold at this level of theory. Possibly, this would require a higher level of correlation to describe long-range "attractive" 1,4 C···C interactions (between equatorial carbonyls of nearby metals).

Electron Density Distribution in $[Cr_2(\mu_2\text{-H})(CO)_{10}]^-$. The "experimental" static deformation density is defined as the difference between the static multipole model density (of the molecule extracted from the crystal) and that of the corresponding promolecule, based on isolated spherical atoms.[47] Showing the redistribution of charge due to atom−atom interactions (both intra- and intermolecular) such deformation density can be used to highlight bonding features whenever spherical atoms, rather than preformed fragments or hybridized atoms, are the correct reference state. In Figure 1b we report the deformation density in the Cr(1)−H−Cr(2) plane highlighting (i) the lobes of electronic charge deficit (negative deformation density) of the metals directed toward the electron-rich hydrogen atom and (ii) the smooth polarization of the hydrogen electron density toward the middle of the Cr(1)···Cr(2) vector rather than toward the Cr atoms. From this point of view the Cr−H−Cr looks like a delocalized donor−acceptor σ-interaction perhaps with a significant electrostatic component. However, no further insight is allowed in the absence of a more accurate QTAM investigation of the total electron density.

In this respect, the first important feature is the *molecular graph*, i.e. the topology of the bond paths (*bp*)[48] and their shapes. Both the experimental and the theoretical charge densities afford

(40) The data in Figure 3 are somewhat scattered; however, a definite correlation between the Cr···Cr distance and the Cr−H−Cr and C_{eq}−Cr−Cr−C_{eq} angles emerges. Actually, at "short" Cr···Cr distances the Cr−H−Cr angle is heavily bent, and the carbonyls prefer a staggered conformation while increasing the Cr···Cr distance flattening of the Cr−H−Cr angle and eclipsing of the $Cr(CO)_5$ moieties are observed.

(41) Richardson, N. A.; Xie, Y.; King, R. B.; Schaefer, H. F., III. *J. Phys. Chem. A* **2001**, *105*, 11134−11143.

(42) Bürgi, H. B.; Dunitz, J. D. *Acc. Chem. Res.* **1983**, *16*, 153−161.

(43) As reported in ref 41, we also found several problems in computing correctly the lower frequency, unless using finer grid for numerical evaluation of the integrals was used. Using the highest accuracy, at the B3LYP/*ae* level the minimum would actually be of C_1 symmetry (somewhat intermediate between C_s and C_2). At BP86 level, the C_s conformer is quite undisputably a local (and absolute) minimum on the PES.

(44) At the B3LYP level, the three conformers collapse into the D_{4h} one.

(45) A full investigation of interconversion paths is, however, beyond our computational availabilities; therefore, we have not performed the theoretical investigations to prove this hypothesis.

(46) At the BP86/*ae* level, although being the highest energy conformer, the D_{4h} is a true minimum on the PES, while at BP86/ecp it is a second-order saddle point. Nevertheless, in both circumstances, the lowest or negative frequency modes are associated with the two paths described.

(47) Coppens, P.; Becker, P. J. In *Mathematical, physical and chemical tables*; Wilson, A. J. C., Prince, E., Eds.; International Tables for Crystallography, Vol. C; Published for the International Union of Crystallography by Kluwer Academic: Dordrecht, Boston, 1995; p 628.

(48) A chemical bond is associated with a line of maximum electron density, called the *bond path* (*bp*), which connects two bonded atoms. The atoms are characterised as maxima of $\rho(\mathbf{r})$ and are defined in space by an atomic basin. A saddle point of $\rho(\mathbf{r})$ along the bond path is called the *bond critical point* (*bcp*, $\mathbf{r_b}$).

Table 3. Summary of the Main Geometrical Features of $[Cr_2(\mu_2\text{-H})(CO)_{10}]^-$ as $[K(crypt\text{-}222)]^+$ Salt and in the Stationary Points Optimized at BP86 Level

	$[K(crypt\text{-}222)]^+$			BP86/*ecp*					BP86/*ae*	
symmetry	$\sim C_s$	C_s	C_2	C_{2v}	C_{2v}	D_{4d}	D_{4h}	C_s	D_{4d}	D_{4h}
relative energy (kcal/mol)	-	0.0	0.041	1.530	1.587	1.270	1.854	0.0	0.640	1.727
nr. of imag. freq.[a]	-	0	1 (*4*)	1 (*11*)	2 (*10*, *14*)	2 (*214*)[b]	2 (*89*)[b]	0	2 (*96*)[b]	0
⟨Cr−H⟩ (Å)	1.73	1.768	1.768	1.776	1.775	1.753	1.765	1.769	1.752	1.767
Cr···Cr (Å)	3.305	3.275	3.277	3.400	3.406	3.506	3.530	3.326	3.504	3.534
$Cr-C_{eq}$ (Å)	1.900	1.876	1.876	1.876	1.875	1.876	1.876	1.896	1.895	1.896
$Cr-C_{ax}$ (Å)	1.847	1.825	1.825	1.822	1.822	1.825	1.823	1.844	1.844	1.842
$\langle Cr-Cr-C_{ax}\rangle$ (deg)	174.3	173.	173.	176.1	180.	180.	180.	173.7	180.	180.
$C_{eq}-Cr-Cr-H$ (deg)		0.; 45.	22.7	0.	45.	-	-	0.; 45.	-	-
$\langle C_{eq}-Cr-Cr-C_{eq}\rangle$ (deg)	19.	45.	45.3	0.	0.	45.	0.	45.	45.	0.
Cr−H−Cr (deg)	145.2	135.7	135.8	146.3	147.3	180.	180.	140.3	180.	180.

[a] Imaginary vibration frequencies are reported in parentheses; [b] Degenerate vibration mode

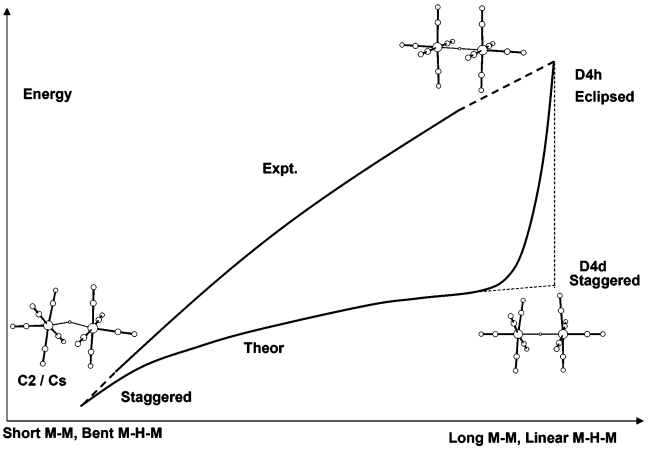

Figure 3. Main stationary points on the PES of $[Cr_2(\mu_2\text{-H})(CO)_{10}]^-$ (see Table 3 for the relative energies involved). See Supporting Information for graphic comprising all stationary points.

molecular graphs lacking a direct metal−metal bond path (see Figure 1c) as previously observed for metal−metal bonds bridged by a symmetric CO ligand.[2] The shape of the outwardly curved, M−H bond paths is however different from that of the inwardly curved M−C ones in M−CO−M systems.[49] An inward curvature of M−C bond paths was considered (for symmetrically bridged carbonyl systems) to be reminiscent of a *closed* three-center bond.[2] Thus, regardless of the actual number of electrons involved, the outward curvature of M−H speaks instead for the presence of an *open* Cr−H−Cr interaction (see Chart 1); this in contrast with the above-mentioned geometrical evidences.

The shape itself of the atomic basins should also be taken into account. Recent studies have investigated more deeply the correlation between the curvature of interatomic surfaces and the bond polarity.[50] In $[Cr_2(\mu_2\text{-H})(CO)_{10}]^-$, regardless of the Cr−H−Cr bond angle, the curvature of Cr−H surface always affords a convex atomic basin for H, although associated with a net negative charge ($q = -0.31$, from BP86/*ae*; $q = -0.28$, experimentally). At qualitative level, all Cr−H−X systems share similar interatomic surfaces, even when hydrogen is substantially neutral as in $[CH_3(\mu_2\text{-H})Cr(CO)_5]$, vide infra.

According to QTAM, the properties of the electron density evaluated at the *bcp* are fingerprints revealing the nature of the atomic interaction. Strong electron-sharing character is associated with a high electron density at the *bcp* and local concentration of the charge ($\nabla^2\rho(\mathbf{r}_b) < 0$). Interactions between closed-shell atoms instead have opposite features. However, bonds involving heavy atoms have different Laplacian distributions because their valence shell is normally "hidden" in the anomalous distribution of shell maxima and minima of the atomic $\nabla^2\rho(\mathbf{r})$ function.[51] For these interactions, the shared or closed shell character is not easily assigned on the basis of charge concentration arguments only. Additional tools for characterizing the "covalence" of bonds are the potential, kinetic, and total energy densities,[52] the (interatomic) delocalization index δ,[53] and the electron density integrated on the interatomic surface, $\oint_{A\cap B}\rho(\mathbf{r})$, which is more informative than just the electron density evaluated at the *bcp*.

From the data in Table 4, which reports a summary of the QTAM analysis on the experimental and theoretical charge densities of the $[Cr_2(\mu_2\text{-H})(CO)_{10}]^-$ anion (in the experimental geometry), it is clear that all Cr−C and C−O bonds behave as in reference metal−carbonyl complexes (see ref 2 for a more comprehensive discussion). If considered separately, each of the two Cr−H interactions results are of course weaker than that of a single terminal hydride, see for example the Mn−H bond characterized experimentally in *cis*-$Mn(CO)_4HPPh_3$[54] or the theoretical calculation on $[CrH(CO)_5]^-$ reported in Table 5. Nevertheless, terminal and bridged-M−H interactions share the signs of the Laplacian and of the total energy density

(49) The take off angles at Cr atoms (i.e. the angles between the bond path and the interatomic vector) always address a path curvature away from the hypothetical Cr−H−Cr ring: 7° and 14° (experimentally); 9° and 16° (at BP86/*ae* level on experimental geometry). However, both Cr−H bond paths show a sudden inward curvature in the vicinity of the H atom, which reduces the Cr−H−Cr bond path angle to 126.7° (experimentally) and 140.7° (at BP86/*ae* level).

(50) (a) Pendás, A. M.; Luaña, V. *J. Chem. Phys.* **2003**, *119*, 7633−7642. (b) Pendás, A. M.; Luaña, V. *J. Chem. Phys.* **2003**, *119*, 7643−7650.

(51) (a) Sagar, R. P.; Ku, A. C. T.; Smith, V. H.; Simas, A. M. *J. Chem. Phys.* **1988**, *88*, 4367−4374. (b) Shi, Z.; Boyd, R. J. *J. Chem. Phys. J. Chem. Phys.* **1988**, *88*, 4375−4377.

(52) At the critical point, covalent interactions are characterized by local excess of potential energy density ($V(r)$, everywhere negative) over the kinetic energy density ($G(r)$, everywhere positive). Thus, the total energy density, $H(r) = G(r) + V(r)$, is negative at the *bcp*, and the ratio $G(r_b)/\rho(r_b)$ is small.

(53) (a) Bader, R. F. W.; Stephens, M. E. *J. Am. Chem. Soc*. **1975**, *97*, 7391−7399. Through a partitioning of the pair density distribution a *localization index* (number of electron pairs localized inside an atomic basin) and a *delocalization index* (number of electron pairs delocalized between two atoms, hereinafter δ(A,B)) are defined. At the HF level of theory, δ(A,B) are in almost exact agreement with the Lewis theory, while post-HF correlated calculations show some significant reduction of the bonded electron pairs compared to the expectations of electron counting rules ((b) Fradera, X.; Austen, M. A.; Bader R. F. W. *J. Phys. Chem. A* **1999,** *103*, 304−314). By its definition δ(A,B) is not restricted to atoms sharing a common interatomic surface and therefore is an indicator able to depict the "electronic communication" between atoms.

(54) Abramov, Y.; Brammer, L.; Klooster, W. T.; Bullock, R. M. *Inorg. Chem.* **1998**, *37*, 6317−6328.

Table 4. Summary of the QTAM Analysis at the Bond Critical Point (bcp) of the Main Interactions in $[Cr_2(\mu_2\text{-}H)(CO)_{10}]^-$ from the Experimental Multipolar Density and the BP86/*ae* Density on the Experimental Geometry[a]

bond A–B		d_{A-B} Å	d_{A-bcp} Å	d_{bcp-B} Å	$\rho(\mathbf{r})$ e Å^{-3}	$\nabla^2\rho(\mathbf{r})$ e Å^{-5}	$G(r)/\rho(\mathbf{r})$ h e^{-1}	$H(r)/\rho(\mathbf{r})$ h e^{-1}
Cr−H	expt.	1.734	1.051(6)	0.684(10)	0.479(8)	5.70(12)	1.05	−0.21
		1.728	1.045(6)	0.686(10)	0.446(8)	6.29(12)	1.13	−0.14
	theor.	1.734	1.059	0.676	0.467	4.20	0.86	−0.23
		1.728	1.054	0.675	0.469	4.34	0.88	−0.23
⟨Cr−C_{ax}⟩	expt.	1.847[3]	0.932[6]	0.916[2]	0.87[1]	14.34[9]	1.502[1]	−0.34[1]
	theor.	1.847[3]	0.939[1]	0.908[1]	0.883[3]	11.3[1]	1.27[1]	−0.378[1]
⟨Cr−C_{eq}⟩	expt.	1.900[5]	0.95[1]	0.94[1]	0.81[3]	12[1]	1.40[5]	−0.34[2]
	theor.	1.900[5]	0.954[2]	0.946[3]	0.779[7]	10.4[2]	1.26[1]	−0.324[4]
⟨C_{ax}−O_{ax}⟩	expt.	1.161[1]	0.382[1]	0.778[1]	2.99[9]	22[3]	2.01[2]	−1.50[6]
	theor.	1.161[1]	0.398[1]	0.761[1]	3.10[1]	0.3[3]	1.850[9]	−1.843[2]
⟨C_{eq}−O_{eq}⟩	expt.	1.150[2]	0.379[2]	0.771[3]	3.12[4]	22[4]	2.04[6]	−1.55[4]
	theor.	1.150[2]	0.395[1]	0.755[2]	3.18[2]	2.2[4]	1.91[1]	−1.860[3]

[a] Experimentally, $H(r)$ and $G(r)$ are computed according to the algorithm proposed by Abramov.[65] Numbers in brackets are standard deviations from the mean for all the parameters that have been averaged. Standard uncertainties are reported for the experimentally derived parameters of the two (unique) Cr−H bonds (actually these values represent a lower limit of the standard uncertainties, because some uncertainties of the refined parameters are not taken into account in the propagation of the error due to a software limitation). As H atoms were not refined in the X-ray study, the standard uncertainties of the two Cr−H distances are omitted.

Table 5. Summary of the QTAM Analysis for Y−H Interactions (in Y−H−X and Y−H Systems) from the BP86/*ae* Densities on the Ground-State Optimized Geometries

Y-H-X	d	d_{Y-bcp}	d_{bcp-H}	Y-H-X	Y···X	$\rho(\mathbf{r})$	$\nabla^2\rho(\mathbf{r})$	$G(\mathbf{r})/\rho(\mathbf{r})$	$H(\mathbf{r})/\rho(\mathbf{r})$	$\int_{\partial\cap B}\rho$	ε	δ_{X-H}	δ_{X-Y}	q(H)
	Å	Å	Å	(°)	Å	e Å^{-3}	e Å^{-5}	h e^{-1}	h e^{-1}	e Å^{-1}				e
$[(CO)_5\mathbf{Cr\text{-}H}]^-$	1.650	1.028	0.622	-	-	0.626	3.58	0.754	-0.354	1.595	0.06	0.59	-	-0.25
D_{4h} $[(CO)_5\mathbf{Cr\text{-}H}\text{-}Cr(CO)_5]^-$	1.767	1.063	0.704	180	3.534	0.415	4.24	0.901	-0.184	1.410	0.0	0.38	0.07	-0.37
C_s $[(CO)_5\mathbf{Cr\text{-}H}\text{-}Cr(CO)_5]^-$	1.769	1.072	0.698	140.3	3.326	0.437	3.89	0.834	-0.209	1.590	0.02	0.38	0.09	-0.31
$[(CO)_5\mathbf{Cr\text{-}H}\text{-}BH_3]^-$	1.752	1.055	0.697	131.5	2.815	0.445	4.59	0.919	-0.196	1.420	0.04	0.38	0.07	-0.44
$[(CO)_5\mathbf{Cr\text{-}H}\text{-}SiH_3]$	1.726	1.045	0.681	112.4	2.776	0.466	5.48	1.027	-0.203	1.70	0.02	0.43	0.13	-0.56
$[(CO)_5\mathbf{Cr\text{-}H}\text{-}CH_3]$	2.009	1.190	0.830	120.5	2.761	0.211	2.73	0.955	-0.047	0.891	0.27	0.13	0.11	-0.04
$[H_3\mathbf{B\text{-}H}]^-$	1.244	0.543	0.701	-	-	0.993	-3.48	0.73	-0.976	1.689	0.0	0.58	-	-0.64
	1.321	0.565	0.844	83.8	1.764	0.844	-0.38	0.828	-0.860	1.337	0.74	0.37	0.12	-0.56
$[H_3\mathbf{B\text{-}H}\text{-}BH_3]^-$	1.322	0.561	0.761	126.6	2.361	0.699	1.44	0.955	-0.811	1.510	0.20	0.35	0.06	-0.57
$[H_3\mathbf{B\text{-}H}\text{-}Cr(CO)_5]^-$	1.330	0.575	0.756	131.5	2.815	0.708	-0.11	0.815	-0.826	1.667	0.29	0.36	0.07	-0.44
$[H_3\mathbf{Si\text{-}H}]$	1.491	0.738	0.753	-	-	0.800	2.28	0.868	-0.669	1.477	0.00	0.59	-	-0.62
$[H_3\mathbf{Si\text{-}H}\text{-}Cr(CO)_5]$	1.590	0.783	0.812	112.4	2.776	0.631	0.86	0.44	-0.381	0.909	0.18	0.43	0.13	-0.56
$[H_3\mathbf{C\text{-}H}]$	1.096	0.694	0.403	-	-	1.837	-22.62	0.161	-1.023	1.780	0.0	0.98	-	0.003
$[H_3\mathbf{C\text{-}H}\text{-}Cr(CO)_5]$	1.122	0.699	0.423	120.5	2.761	1.681	-18.81	0.190	-0.973	2.04	0.003	0.87	0.11	-0.04
$[\mathbf{H\text{-}H\text{-}H}]^{+}$ [(a)]	0.829	0.328	0.501	180.0	1.658	1.161	-18.05	0.0	-1.264	0.823	0.0	0.48	0.15	-0.21
$[\mathbf{H\text{-}H\text{-}H}]^{-}$ [(a)]	1.062	0.573	0.489	180.0	2.124	0.788	-5.00	0.168	-0.619	0.905	0.0	0.54	0.35	0.12

[a] For both H_3^+ and H_3^- the linear symmetric geometry is not a minimum on the PES. H_3^+ equilibrium geometry is D_{3h}, while H_3^- is $C_{\infty h}$.

evaluated at the bcp. This is not unexpected, considering the relatively small elongation of the Cr−H distance in the bridging system. Moreover, judging from $\rho(\mathbf{r})$, a kind of cooperative effect is at work in the Cr−H−Cr moiety; in fact the two Cr−H are not just "half-bonds", although this is not quantifiable unambiguously.[55]

We may expect further insight on the dichotomy implied in Chart 2 from the analysis of the shape of the Laplacian distribution ($\nabla^2\rho(\mathbf{r})$), that is known to enhance the features of charge density and of electron pair localization, providing a physical connection with the classical Lewis model and the valence shell electron pair repulsion theory.[56] Here, the bridging hydride is surrounded by a unique valence shell charge concentration, polarized toward the Cr- - -Cr midpoint (see Figure 1d). This shell is, however, too small to contain the Cr−H critical points which are then associated with a positive value of the Laplacian (see Table 4). Noteworthy, around the Cr atoms we observe a cubic disposition of the valence shell charge concentrations (VSCC's),[57] as expected for an octahedral coordination which, however, is not significantly perturbed by the off-axis location of the hydride (see Figure 4). This is consistent with the hypothesis that the metal σ-orbitals most suitable to interact with the hydride are in fact directed along the axial ligand metal vectors. Nevertheless, these arguments do not allow ascertaining the presence of some Cr- - -Cr direct contribution and therefore discriminating between different bonding models for the M−H−M system. More insight must

(55) Electron density at bcp's strongly depend on the equilibrium geometry, which is quite affected by the total molecular charge; therefore, geometry comparisons of moieties contained in $[Cr_2(\mu_2\text{-}H)(CO)_{10}]^-$ and in $[CrH(CO)_5]^-$ are somewhat inappropriate.

(56) Gillespie, R. J.; Hargittai, I. *The VSEPR Model of Molecular Geometry*; Allyn and Bacon: Boston, MA, 1991.

(57) Bader, R. F. W.; Gillespie, R. J.; MacDougall, P. J. *J. Am. Chem. Soc.* **1988**, *110*, 7329−7336.

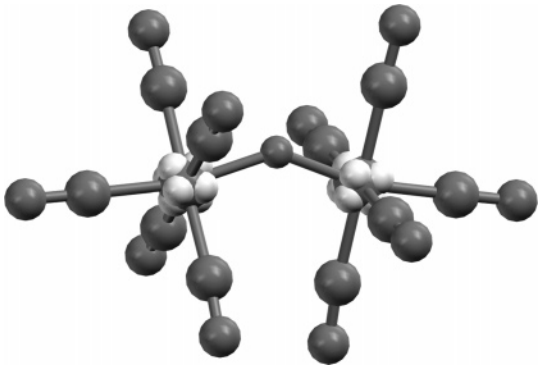

Figure 4. VSCC's (light gray balls) around Cr atoms in the C_s conformer of $[Cr_2(\mu_2\text{-H})(CO)_{10}]^-$. The stereochemistry imposed by CO ligands is clearly overwhelming the H shift out of axial position; it is clear that CO are disposed according to the faces of the cubic disposition of VSCC's without significant distortion [as in the "parent" $Cr(CO)_6$]

then be retrieved from additional topological features of the electron and pair density distribution.

As we extensively pointed out in previous works,[2] the analysis of only the electron density might not disclose all the features of a bonding status, especially in the presence of multicenter bonding. Instead, the access to at least some features of the pair density distribution[58] can give a more comprehensive view, which better explains also the features of the PES (for example, its flatness along some stereochemical rearrangement coordinate). In this respect, the most useful indicator is the delocalization index (δ),[53] that is a measure of the degree of electron sharing between two atoms (either connected or not by a bond path). It is interesting to note that the Cr−H delocalization in the Cr−H−Cr system is somewhat larger than one-half of that of single Cr−H (as in $[CrH(CO)_5]^-$) and that a significant Cr- - -Cr delocalization is present also in the D_{4h} conformer, that is when no possible direct metal−metal bond can be argued (see Table 5). In other words, the degree of three-center bonding is quite large in this system, and therefore, it produces some metal−metal electron sharing even in the absence of a direct interaction. In the bent C_s isomer (where a direct bonding would, in principle, be possible) δ(Cr,Cr) is only slightly larger, despite its stereochemistry, and the shorter Cr- - -Cr distance would suggest a stronger enhancement. At the same time, no indicator reveals a weakening of the Cr−H bond on passing from linear D_{4h} to bent C_s conformation. Indeed, we note that the electron density at the critical points and on the whole interatomic surfaces shared by each Cr and the H increases, the delocalization remains almost unchanged, and as noted before, the bond path lines are not deflected toward the ideal Cr- - -Cr line. There is an additional surprising observation, namely the large delocalization between the hydrogen and the equatorial carbonyls. This feature is particularly clear by inspection of the Fermi hole[1] map of the C_s conformer, where the delocalization with the three nearby equatorial carbonyls is particularly strong (hence, graphically visible). Positioning the probe electron at each of the two Cr−H critical points, we observe the polarization of the Fermi hole density toward the nearest CO (see Figure 5). At the same time, we can clearly appreciate the delocalized nature inside the Cr−H−Cr region, because the Fermi hole picture is substantially unmodified on moving the probe electron along the entire Cr−H−Cr bond paths within the H atomic basin (Figure 5). The interaction of the hydride and the eclipsed carbonyl is, of course, weakened on passing from C_s (d_{H---C} = 2.275 Å, δ(C,H) = 0.08) to D_{4h} (d_{H---C} = 2.583 Å, δ(C,H) = 0.05); accordingly, the overall sum of H- - -CO delocalization indexes also slightly decreases (the averaged H- - -C_{eq} distances are 2.571 and 2.583 Å respectively).[59] Of course, this might be just one of the concurrent electronic and sterical effects causing the C_s conformer (with bent Cr−H−Cr and off-axis position of the H) to be the geometry of minimum energy on the $[Cr_2(\mu_2\text{-H})(CO)_{10}]^-$ PES; nevertheless, it does not seem negligible, and it allows prediction of alternative configurations in this family of complexes (see below).

Electron Density Distribution in [Cr−H−X] systems. Whenever a new interaction within the realm of organometallic compounds is investigated by QTAM, we must inductively derive the "correspondence rules" between fuzzy, but assessed, chemical insight and precise topological entities.[2] To develop further analogies for the M−H−M bond we have therefore studied a series of $Cr(CO)_5H-X$ complexes and, for sake of comparison, the corresponding X−H−X systems.

Inspection of Table 5 shows the impressive similarities between $[(CO)_5Cr-H-Cr(CO)_5]^-$, $[(CO)_5Cr-H-BH_3]^-$, and $[H_3B-H-BH_3]^-$. In fact, the $(CO)_5$**Cr**−**H**−X and H_3**B**−**H**−X topological features do not change on passing from X = $Cr(CO)_5$ to X = BH_3 in keeping with their geometries and shape of the atomic basins (compared in Figure 6). On passing to neutral complexes, one notes that for X = SiH_3 the Cr−H bond is slightly reinforced, whereas for X = CH_3, it is definitely weaker.

If the X counterpart is stereo-electronically different, then the Cr−H−X system becomes definitely asymmetric. This can be visualized by the absolute difference between bond distance variations from the isolated $(CO)_5Cr-H$ and H−X molecules:

$$\eta(\text{dist}) = |d_1/d_2 - d_3/d_4|$$

where d_1 and d_3 are distances of the Cr−H and H−X bonds in their isolated molecules and d_2 and d_4 are their corresponding distances in the Cr−H−X system.

Using η(dist), $(CO)_5Cr-H-Cr(CO)_5$ and $(CO)_5Cr-H-BH_3$ look similar, and their symmetry is evident, whereas $(CO)_5Cr-HCH_3$ is clearly the most asymmetrical (η = 0.17) complex. Of course, one could instead use the delocalization indexes and compute the η (δ) parameter:

$$\eta\,(\delta) = |\delta_2/\delta_1 - \delta_4/\delta_3|$$

Again, $(CO)_5Cr-HCH_3$ would appear as a highly asymmetric Cr−H−X system (η = 0.67), while η is close to zero for $[(CO)_5Cr-HBH_3]^-$ and $(CO)_5Cr-HSiH_3$, indicating an almost perfect replacement of one $Cr(CO)_5$ moiety. Interestingly, higher symmetry is associated with larger stability of the complexes (see Table 6).

Apart from the role of the ancillary ligands, which assist only the "metallic hydridic fragment", the nature of the chemical bonding is roughly similar in all these systems, either symmetric or not. We may even think of a hypothetical continuum joining

(58) McWeeny, R.; Sutcliffe, B. T. *Methods of molecular quantum mechanics*; Academic Press: London, 1969.

(59) Also a more classical indicator, like the overlap population, addresses the importance of these interactions. For example, the overlap population of the shortest C- - -H contact in the C_s conformer is ca. 15% of the Cr−H one, and it decreases on going to the linear eclipsed conformer, in analogy with the behavior of the corresponding delocalization index.

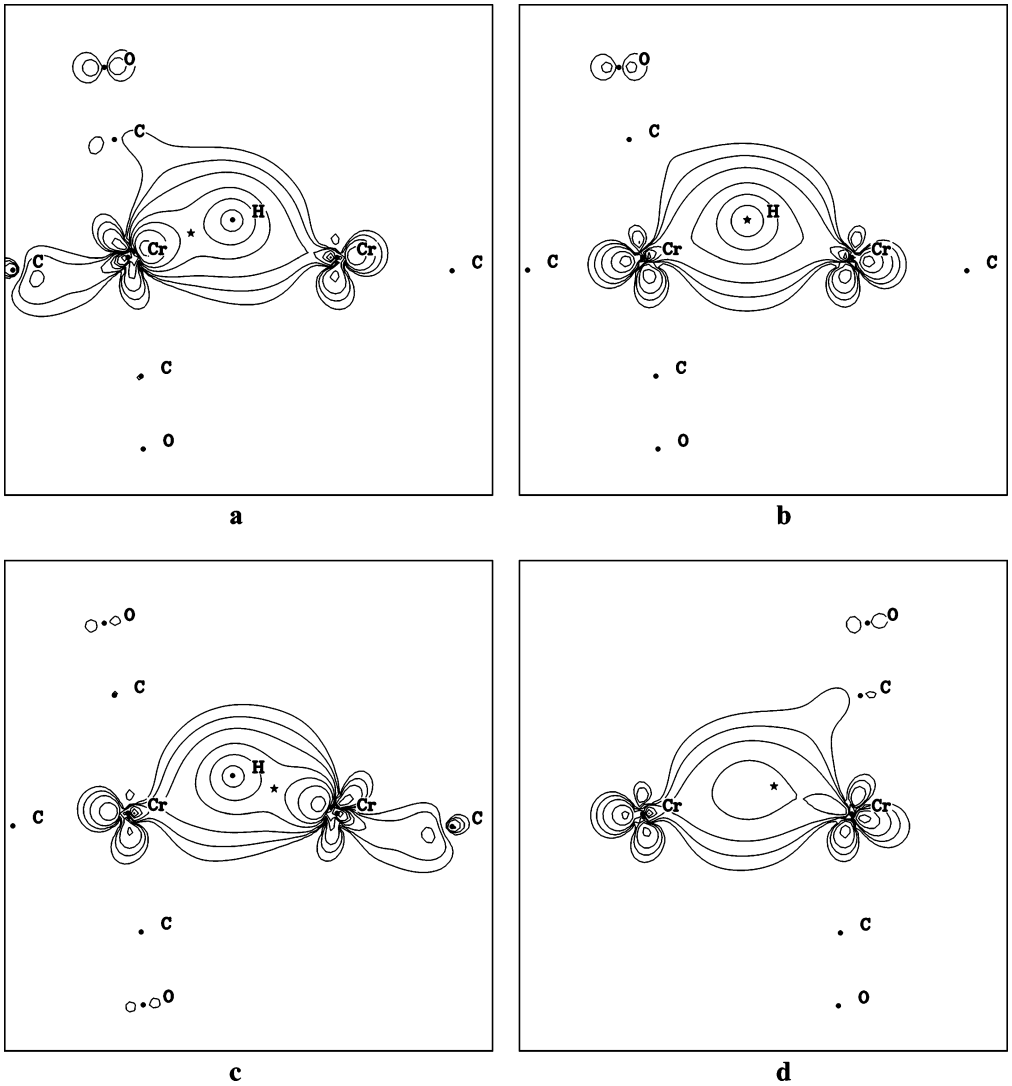

Figure 5. Fermi hole density distribution in the C_s conformer of $[Cr_2(\mu_2\text{-H})(CO)_{10}]^-$. (a−c) In the plane defined by the Cr atoms and the hydride; (d) in the plane orthogonal to the previous one and containing the Cr atoms. The position of the reference electron, located at bcp's (a, c, and d) and at the H site (b), is marked by a star.

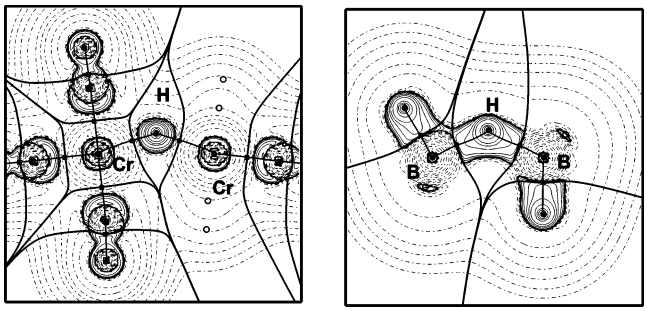

Figure 6. Laplacian distribution of $[Cr_2(\mu_2\text{-H})(CO)_{10}]^-$ and $[B_2H_7]^-$ in C_s conformation, computed at BP86/*ae* level. Bond paths and projection of the interatomic surfaces are superimposed.

the extremes, which are characterized by $\eta = 0$ and $\eta \rightarrow 1$. This can lead to the conclusion that the Cr−H−Cr (or the B−H−B) is nothing else but a *symmetric agostic interaction*, stabilized by the identity between X and Y in the Y−H−X system. This reasoning is somewhat analogous to the symmetric single-well X−H−X hydrogen bond compared to the asymmetric double-well X−H−Y counterpart.[60] The agostic type X−H···M interaction is typical of stronger X−H bonds, likewise for C−H (for which the definition itself was introduced[61]) leading to highly asymmetric systems, where the M- - -C or M- - -H interactions are modest and almost indistinguishable (in case of d^0 metals, the stabilizing contributions do not even depend on σ-donation of the X−H bond).[62] Indeed, in $(CO)_5Cr-H-CH_3$ electron delocalization between Cr and H is almost identical to that between Cr and C (see Table 5).

On the other hand, in symmetric systems the H−X and H−Y bonding contributions are clearly overwhelming the X- - -Y interaction (a feature typical of three-center-two-electron bonds). The analogy with the hydrogen bond (i.e. the prototype of three-center-four-electron bonds) may suggest further investigation of the equilibrium geometry in asymmetric species. In fact, one might suppose that the observed minimum might not be unique on the PES. For sake of simplicity, we made explorative calculation on $H_3B-H-CH_3$, that could be considered analogous to $(CO)_5Cr-H-CH_3$, given the similarity between BH_3

(60) Gilli, P.; Gilli, G. *J. Mol. Struct.* **2000**, *552*, 1−15.

(61) (a) Brookhart, M.; Green, M. L. H. *J. Organomet. Chem.* **1983**, *250*, 395−408. (b) Brookhart, M.; Green, M. L. H. Wong, L. L. *Prog. Inorg. Chem.* **1988**, *36*, 1−124.

(62) Scherer, W.; McGrady, G. S. *Angew. Chem., Int. Ed.* **2004**, *43*, 1782−1806 and references therein.

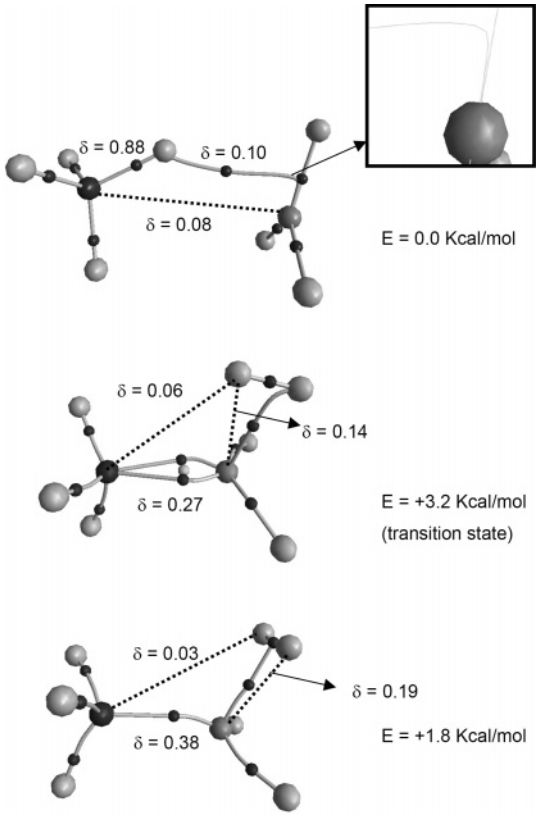

Figure 7. Main stationary points found on the PES of CH_4BH_3. Pertinent delocalization indexes are reported. Dotted lines identify interactions which are not associated with bond paths.

and $Cr(CO)_5$ demonstrated above. Indeed, the "agostic" H_3B- - -H−CH_3 complex is not the only minimum on the PES, where we also found a $(H_4B)^-$- - -$(CH_3)^+$ isomer, that actually carries an η^2 H−H bond at the B atom (see Figure 7 for a schematic resume of geometries, topologies, energies, and δ's in the two conformers and in the transition state).[63] The energy difference is quite small (1.8 kcal/mol), and it clearly suggests that an interplay between the two configurations is always occurring along the PES of this complex. In H_3B−H−CH_3, the presence of "hydridic" hydrogens allows the formation of the H−H complex on the B side, stabilizing the second well of this double-well potential. The strong interaction between the hydride bridge and the ancillary ligands described in the previous section is in perfect agreement with the alternative minimum found on H_3B−H−CH_3 PES and with previous experimental and theoretical investigations on the dynamics of dimetallic hydrides.[63]

The strength of the hydride bridge interaction may be quantified investigating how it affects the coordination of the other ligands to the metal. In octahedral $M(CO)_5L$ complexes, the difference between equatorial and axial metal−carbonyl bond lengths (Δd) is an indirect measure of the strength of the M−L bond itself. In $Cr(CO)_6$ (where L = CO), all M−CO's are quite elongated because each carbonyl is trans to another. On the other hand, a weaker ligand produces a shorter M−C(axial) distance (without affecting the equatorial carbonyls). Consequently, Δd is positive, and roughly, the larger the Δd the weaker is the ligand L.

Table 6. Binding Energies and Asymmetric Parameters of Some Y−H−X Complexes Investigated in the Text

complex	binding energy[a] (kcal/mol)	η (dist)	Δd (Å)[b]
$[Cr_2(\mu_2\text{−H})(CO)_{10}]^-$	−40.7	0	−0.054
$[B_2H_7]^-$	−37.8	0	-
$[Cr(CO)_5HBH_3]^-$	−29.1	0.01	−0.049
$Cr(CO)_5HSiH_3$	−16.5	0.02	−0.038
$Cr(CO)_5HCH_3$	−5.4	0.17	−0.069
BH_3HCH_3	−0.8	0.32	−

[a] Computed respect to the more stable fragmentation (X + H−Y or X−H + Y), without including correction for basis set superposition error and zero-point vibration. [b] Δd is the difference between the OC−Cr bond distance trans to the Cr−H bond and the averaged Cr−CO bond distances of the four equatorial carbonyls.

Comparing the Δd in $Cr(CO)_5HX$ systems (Table 6), we found that the $[HCrCO_5]^-$ moiety has a lower trans influence (i.e., a larger Δd) than H^- (whose Δd is close to 0.0). Moreover, Δd increases as the binding energy of the HX fragment decreases. For example, in $Cr(CO)_5HCH_3$ Δd is even larger and quite close to that observed for the $Cr(CO)_5$ in C_{4v} symmetry that, lacking the trans ligand, has the highest Δd. $Cr(CO)_5HCH_3$ is in fact very loosely bound.

Conclusions

In this work we have analyzed the theoretical electron density distribution of some M−H−X systems and compared that of the $[Cr_2(\mu_2\text{-H})(CO)_{10}]^-$ anion to the experimental one determined on its $[K(crypt\text{-}222)]^+$ salt. We confirmed the flatness of its PES which implies that large conformational variations correspond to small energy changes. Therefore, even if in the gas phase only the C_s conformer lies in a minimum, many others could be found in different, more perturbing, environments. In fact, the comparative study of the many $[Cr_2(\mu_2\text{-H})(CO)_{10}]^-$ salts characterized thus far confirms this picture and allows the definition of an "experimental" interconversion path (Figure 2) between the two conformers, C_s and pseudo-D_{4h} (C_{2v}), representative of the staggered and eclipsed structures, respectively. This transformation could be explored also in terms of the topology of the electron density. Inspection of Table 7 does not address a "unique effect" stabilizing one isomer over the other. The electron density integrated on the interatomic (Cr|H) surfaces seems to favor the Cr−H interactions in the staggered geometry, but this is contradicted by the Cr−H delocalization indexes. On the basis of this analysis one can be tempted to credit the significant role of "packing forces" in determining the solid-state conformation of such an anion. However, some general features emerge anyway. For example, the shift of the H atom out of the idealized $(OC)_{ax}$−M direction seems to be a constant in M−H−M systems that cannot be attributed just to the increase of M- - -M direct interaction. Indeed, the role of the nearby equatorial carbonyls is manifest in the Fermi-hole density distribution and in the corresponding H- - -CO delocalization indexes.

We have also compared the Cr−H−X bonding in some systems, finding an impressive similarity between $Cr(CO)_5$ and BH_3 moieties which classically can be considered as isolobal.[64,65] In the QTAM frame, this results in the very similar electron

(63) Evidence of a similar η-H_2 intermediate was obtained in the (DFT and NMR) study of the mutual exchange between terminal and bridging hydrides in $Re_2H_2(CO)_9$ (see Bergamo, M.; Beringhelli, T.; D'Alfonso, G.; Mercandelli, P.; Sironi, A. *J. Am. Chem. Soc.* **2002**, *124*, 5117−5126).

(64) Hoffmann, R. *Angew. Chem., Int. Ed. Engl.* **1982**, *21*, 711−724.
(65) Abramov, Y. A. *Acta Crystallogr.* **1997**, *A53*, 264−272.

Table 7. Geometric and Electron Density Properties (at BP86/*ae* Level) Evaluated at Cr−H Critical Points and Interatomic Surfaces for the "Experimental" Conversion Path Obtained by Idealizing the Geometries of CSDS Databank (see also Figure 2)[a]

Cr···Cr Å	Cr–H–Cr (deg)	C_{eq}–Cr···Cr–C_{eq} (deg)	$\rho(r)$ e Å^{-3}	$\nabla^2\rho(r)$ e Å^{-5}	$G(r)/\rho(r)$ h e^{-1}	$H(r)/\rho(r)$ h e^{-1}	$\oint_{A\cap B}\rho(\mathbf{r})$ e Å^{-1}	ϵ	δ Cr–H	δ Cr–Cr	relative energy kcal/mol
3.220	137.1	45	0.480	4.15	0.85	−0.25	1.85	0.04	0.370	0.104	0.00
3.250	139.9	39	0.478	4.16	0.85	−0.24	1.79	0.04	0.372	0.103	0.28
3.280	142.9	28	0.475	4.19	0.86	−0.24	1.79[b]	0.04	0.372	0.099	1.07
3.310	146.1	16	0.472	4.21	0.86	−0.24	1.58[b]	0.05	0.373	0.097	2.29
3.340	149.7	6	0.469	4.24	0.87	−0.24	1.52	0.06	0.372	0.093	2.85
3.390	156.9	0	0.461	4.36	0.89	−0.23	1.46	0.04	0.377	0.088	2.48

[a] The two independent Cr−H bonds are averaged. Cr−Cr and Cr−H delocalization indexes are also tabulated. Note that theoretical and experimental geometries differ in Cr−H distances, which explains the discrepancies in electron density properties of Cr−H bonds compared to the gas-phase optimized C_s and D_{4h} conformers reported in Table 5. [b] The highest accuracy failed in evaluating the surface integrals for this geometry, hence the results were produced with lower accuracy.

and pair densities within the M−H−X fragment, also manifested by a similar shape of the H atomic basin.

In addition, although the agostic (M- - - H−C) interaction and the symmetric hydride bridge (M−H−M) present undisputedly different geometries, they share the very same bonding nature (at least as far as σ-donation of C−H occurs). In asymmetric (agostic) interactions, there is a kind of schizophrenic behavior of the metal, whose binding could be directed alternatively to H or X (in the molecular graphs of the most stable conformers of CH_4−BH_3 complex the H- - -B bond is even not so well defined and close to the H- - -H bonding observed in the transition state, see Figure 7). As the M−H and X−H bonds become more similar in strength, then a clear predominance of M−H over M- - - X is observed, and the structure approaches a more symmetric appearance characterized by small M- - -X delocalization. We have proposed a similarity between the three-center-two-electron system here investigated and the most representative example of three-center-four-electron bonding, namely the hydrogen bond. Weaker HBs are often double-well, although characterized by one dominant configuration and lower delocalization. The directionality of the HB is somewhat preserved by the electrostatic component (that is active even in the absence of strong covalency). In M−H−X systems, instead, weaker H-bridges are not particularly assisted by electrostatics (the metal is always positively charged, the hydrogen becomes neutral or even positive as X−H reinforces); therefore, directionality at longer range is lost. Nevertheless, the covalent components of the bonding are similar in symmetric and asymmetric systems, and progress toward symmetric H-bridges is unavoidable as the M−H and X−H bonds become similar.

If compared to the previously studied carbonyl-bridged M−M bonds,[2] we note that the M−H−M systems have undisputedly many subtler features associated with even smaller energy gradients that therefore hamper an easier rationalization of the bonding effects. More than before, a study beyond a "simple" electron density distribution analysis was necessary here to detect minor forces acting for the overall stability of the system.

Acknowledgment. We thank the Italian MURST (PRIN2003, Project "Metal Carbonyl Clusters Functional to NanoMaterials"; FIRB "Intra and Intermolecular Weak Interactions").

Supporting Information Available: Crystallographic data in CIF format; the residual density map from experimental electron density determination; figures of all stationary points identified on the PES of $[Cr_2(\mu_2\text{-H})(CO)_{10}]^-$; and complete ref 24. This material is available free of charge via the Internet at http://pubs.acs.org.

JA055308A